

XMM-Newton view of the Multi-Phase Warm Absorber in Seyfert 1 Galaxy NGC985 ¹

Yair Krongold¹, Elena Jiménez-Bailón¹, Maria Santos-Lleo², Fabrizio Nicastro^{3,4}, Martin Elvis⁴, Nancy Brickhouse⁴, Mercedes Andrade-Velazquez¹, Luc Binette^{1,5} & Smita Mathur⁶

ABSTRACT

We present an analysis of a new *XMM-Newton* observation of the Seyfert 1 Galaxy NGC 985. The *EPIC* spectra present strong residuals to a single power-law model, indicating the presence of ionized absorbing gas and a soft excess. A broad-band fit to the *EPIC* and *RGS* spectra shows that the continuum can be well fit with a power-law ($\Gamma \approx 1.57$) and a blackbody component ($kT \approx 0.09$ keV). The *RGS* can be modeled either with two or three absorption components. In the two absorber model the low-ionization one, with $\log U \approx .05$ and $\log N_H \approx 21.08$ accounts for the presence of the Fe M-shell unresolved transition array (Fe VII-XIII), and the high ionization component ($\log U \approx 1.31$ and $\log N_H \approx 21.99$) is required by the presence of several Fe L-shell transitions. The data suggest the presence of a third ionized component with higher ionization, so that the Fe L-shell absorption features are produced by two different components (one producing absorption by Fe XVII-XX, and the other absorption by Fe XX-XXII). However, the presence of the third absorbing component cannot be detected by means of an isolated absorption line in a significant way, so we consider this detection only as tentative. Interestingly, all ionization components have similar kinematics (with outflow velocities ~ 280 km s⁻¹). In addition, whether two or three absorbers are considered, the components appear to be in pressure balance within 1σ . These results give further support to the idea that warm absorbers

¹Instituto de Astronomia, Universidad Nacional Autonoma de Mexico, Apartado Postal 70-264, 04510 Mexico DF, Mexico.

²ESA XMM-Newton Science Operations Center, ESAC, PO Box 78, E-28691, Madrid, Spain

³Osservatorio Astronomico di Roma, INAF, Italy.

⁴Harvard-Smithsonian Center for Astrophysics, 60 Garden Street, Cambridge MA 02138, USA.

⁵Departement de Physique, de Genie Physique et d'Optique, Universite Laval, Quebec, QC G1K 7P4, Canada

⁶Ohio State University, 140 West 18th Avenue, Columbus, OH 43210, USA.

in AGN consist of a two or three-phase medium. We note that, while in the model with only two absorbers one of them (the high ionization component) lies on an unstable branch of the thermal equilibrium curve, in the model with three absorbers all of the components lie on stable branches of the curve. This gives further plausibility to a multi-phase absorber.

Subject headings: galaxies: absorption lines – galaxies: Seyferts – galaxies: active
– galaxies: X-ray

1. Introduction

Highly ionized (or ‘warm’, WA) absorbers are observed in about half of X-ray spectra of broad line active galactic nuclei (AGN), both Seyfert 1s (e.g. Halpern 1984; Reynolds et al. 1997, George et al. 1998) and quasars (Piconcelli et al. 2005). The absorption lines of these systems are blueshifted with respect to the optical emission lines (with velocities of the order of a few hundreds to $\sim 2000 \text{ km s}^{-1}$), implying outflowing winds. Their frequency, combined with evidence for transverse flows (Elvis 2000; Crenshaw et al. 2003; Arav 2004) suggest that WAs are actually ubiquitous in AGN, but become directly visible in absorption only when our line of sight crosses the outflowing material. Ionized absorption is also observed in the UV band. However, the exact relation between the X-ray absorbers and Narrow Absorption Line (NAL) UV systems is still uncertain. These absorbers must be related, as exactly the same AGNs show both (Mathur et al. 1995), and in many cases, with similar outflow velocities and similar ionization state.

Several studies have shown that the absorbers can be described in a simple way. It has been shown that X-ray ionized absorbers can be well modeled by including only two or three absorbing components (Krongold et al. 2003, 2005a; Netzer et al. 2003; Blustin et al. 2003; Steenbrugge et al. 2005). It has also been found that these components appear to be in pressure balance with each other (Krongold et al. 2003, 2005a, 2007; Netzer et al. 2003). This has been interpreted as evidence of a multi-phase medium for the structure of the absorber. Alternatively, it has also been suggested that we could be looking at a single radially stratified medium with constant pressure (Rozanska et al. 2006). Other studies suggest that the warm absorber could consist of a continuous radial flow of ionization structures (Behar et al. 2003; Ogle et al. 2004; Steenbrugge et al. 2005), though variability studies seem to rule out this

¹Partially based on observations obtained with XMM-Newton, an ESA science mission with instruments and contributions directly funded by ESA Member States and NASA.

possibility (Krongold et al. 2005b, 2007). An intermediate case consisting of a double peaked continuous distribution of material has also been reported for Mkn 279 (Constantini et al. 2007), although Fields et al. (2007) reports that these data is consistent with a multiphase medium, once metalicity effects are taken into account. The exact nature of AGN winds still remains a mystery.

The nature of the wind directly impacts our understanding of both the structure and physics of the active nucleus itself, and the effect of AGNs on their larger scale galactic and extragalactic environment. One of the key questions is where do these absorbers originate. Several studies have set lower limits on the location of the ionized outflows, placing them at parsecs from the central ionizing source (Behar et al. 2003, Netzer et al. 2003), and suggesting an origin in the putative obscuring torus (Krolik & Kriss et al. 2001, Blustin et al. 2005). However, other studies have found WA much closer in, at sub-pc scales (Pounds et al. 2003; Kaastra et al. 2004, Krongold et al. 2007), leading to the suggestion that warm absorbers originate from the accretion disk (Krongold et al. 2007). The mass loss rate inferred for these outflows is still uncertain by orders of magnitude and is strongly debated, as this rate depends critically on the distance of the outflow to the central source.

1.1. The Ionized Absorber in NGC 985

NGC 985 (Mrk 1048) is a Seyfert 1 galaxy located at redshift 0.04274 ± 0.00005 (12814 ± 15 km s⁻¹; Arribas et al. 1999, based on stellar absorption features, see Krongold et al. 2005 for a detailed description of NGC 985).

An ionized absorber has been observed in the X-ray spectra of this object; first through low resolution data (Brandt et al. 1994 in a ROSAT-PSPC spectrum of this source; Nicastro et al. 1998, 1999, with an ASCA observation). High resolution observations carried out with the HETGS on board the *Chandra* X-ray telescope (and performed ~ 1 year before the *XMM-Newton* observations discussed here) have confirmed the presence of the absorber (Krongold et al. 2005 hereafter K05). In this analysis, it was found that two absorbing components were required to fit the spectrum of NGC 985. Furthermore, the gas pressure of the two components was consistent, suggesting that the absorber could be formed by a two-phase wind. The UV band also shows the presence of absorption lines produced by ionized gas (Arav 2002). Five components are observed in outflow, with velocities ranging from 780 to 243 km s⁻¹. A sixth component is observed inflowing at -140 km s⁻¹.

In this paper we present the analysis of the ionized absorber in NGC985 carried out on XMM-Newton X-ray spectra. In §2 we describe the reduction of the data. In §3, we present

the data analysis, including a detailed model of the ionized absorber in NGC 985. In §4 we discuss our results, and compare them with those obtained with the *Chandra* data by K05. Finally, in §5 we present our conclusions.

2. Observations and Data Reduction

The *XMM-Newton* (Jansen et al. 2001) observation of NGC 985 (Obs-Id. 0150470601) was performed on July 17, 2003. Thin filter and small window mode were applied for the *EPIC* (European Photon Imaging Camera) *pn* exposure. The *MOS-1* and *MOS-2* observations were performed with the thick and thin filter and the partial window mode and prime full window mode, respectively. Both *RGS* (Reflection Grating Spectrometer) cameras were in spectroscopic mode. *Science Analysis Subsystem*, SAS, v.7.1.2 (Gabriel et al. 2004) and the most updated calibration files available in March 2008 were used to process the data. According to the *epaplot* task, no sign of pile-up was detected in any of the *EPIC* observations. Time intervals for which background flaring degrades the signal to noise in the *EPIC* observations were excluded from the analysis following the filtering method described in Piconcelli et al. (2004). The exposures after the filtering are 40.3, 47.5 and 57.1 ks for *pn*, *MOS-1* and *MOS -2*, respectively. The exposure for both *RGS* is 57.7 ks.

3. Spectral Analysis

We have performed a spectral analysis of the *EPIC-pn* and *RGS* instruments on board *XMM-Newton*. The circular extraction regions of *EPIC-pn* data were centered on the peak of the X-ray emission and have a radius of $35''.7$ (750 pixels). The background regions were selected to be on the same CCD, but far enough from the source to prevent contamination. *RGS* spectra were extracted using the SAS task *rgsproc* run with default parameters. The *EPIC-pn* data have been studied in the 0.35-10 keV (1-37 Å) band, and the *RGS* in the 0.33-1.77 keV (7.0-38.0 Å) band. In order to apply the modified Chi-Squared minimization technique in the spectral analysis, all *EPIC* data were grouped such that each bin contains at least 20 counts. The *RGS* spectra were fitted with a 10 channel binning (i.e. in bins of size 0.1 Å) using Chi-Squared Gehrels statistics. When grouping the *RGS* data in this way, each channel has at least 20 counts, and thus possible bias introduced by the use of Chi-Squared statistics with low count rate data are avoided (see Wheaton et al. 1995 for the case of Poisson statistics). However, this bin size is about twice the *RGS* FWHM, which leads to a

sensitivity loss to detect weak narrow absorption or emission lines in the spectrum.²

The spectral analysis were performed using the *Sherpa* package³ of *Ciao 3.3* (Freeman et al. 2001). We exploit the PHASE code (Krongold et al. 2003) to model in a self consistent way the ionized absorbers present in NGC 985. We have explored only photoionization equilibrium models and we have assumed solar elemental abundances (Grevesse & Noels 1993). In all the models, we have taken into account Galactic absorption by applying a cold absorption component with an equivalent Hydrogen column frozen to the Galactic value ($N_H=3.0 \times 10^{20} \text{ cm}^{-2}$, Stark et al. 1992).

3.1. Analysis of the *EPIC* data

The *EPIC-pn* data was first analyzed in the hard energy band (2-10 keV). Table 1 shows the values of the continuum parameters and the goodness of the fits for several tested models. A power law model (model A) does not provide an acceptable fit to the data, reduced $\chi^2_\nu = 1.33$ for 174 d.o.f. The most prominent residuals appear around 6-6.3 keV. An emission line improves the fit (model B) with a probability $> 99.999\%$ according to an F-test. The energy of the line, $6.421 \pm 0.025 \text{ keV}$ (see Table 1), is consistent with the neutral FeK α line. The emission line is narrow, $\sigma = 0.14 \pm 0.03 \text{ keV}$. Its properties are compatible with an origin in low ionization material, probably located in the Broad Line Region given the width of $\sim 6500 \text{ km s}^{-1}$ (this width is too broad to suggest an origin in the molecular torus). The equivalent width of the line is $129^{+25}_{-20} \text{ eV}$, compatible within the errors with mean values measured for Type 1 objects (Jiménez-Bailón et al. 2005). These are features commonly found in AGNs with WA.

Although model B provides an adequate fit ($\chi^2_\nu=0.94$ for 171 d.o.f) to the observed data above 2 keV, when the lower energy band is considered the fit is strongly unacceptable. The lower part of Figure 1 shows the residuals of the data to model B in the low energy band. The *pn* data shows positive and negative residuals typical of absorbing features and also hint the presence of a soft excess below 1 keV. A cold absorption component additional to the Galactic one causes no significant improve to the broad-band fit.

²We note however, that a test on our final model (§3.3), using data with a binning size of 0.05 Å (similar to the size of the RGS FWHM), and C-statistics gives results fully consistent with those found in our analysis. This indicates that this sensitivity loss has no effect on our conclusions.

³<http://cxc.harvard.edu/sherpa/>

3.2. Analysis of the RGS data

Based on the results obtained with the *EPIC* data, we have tested for the presence of the ionized absorber in the *RGS-XMM-Newton* high resolution data. The continuum model, consisting of a power law plus a blackbody (as indicated by the *EPIC* data), was first attenuated by one warm absorbing component modeled with PHASE (model C). PHASE has 3 free parameters for each absorbing component: the ionization parameter ($\log U$), the equivalent Hydrogen column density ($\log N_H$) and the outflow velocity (v_{out}) of the absorbing gas. A fourth parameter, the microturbulence velocity of the material (v_{Turb} , which is added in quadrature to the thermal velocity to compute the total Doppler broadening: $v_{DOP}^2 = v_{Therm}^2 + v_{Turb}^2$) is not easily constrained with current grating spectra and, in all the models used here, was set equal to 300 km s^{-1} (see Krongold et al. 2003 for details)⁴.

The spectral energy distribution (SED) used to produce the PHASE models was the same used by K05 (see their Fig. 3a and §2.1.2), based on multi-frequency data of NGC 985 (mostly obtained from the NASA Extragalactic Database, NED)⁵. This SED has a UV break beyond 1200\AA (at 912\AA), and the UV and X-ray continua meet at around 0.1 keV . This shape is consistent with recent results by Haro-Corzo et al. (2006), who studied in detail the shape of the SED from the far UV to the X-rays.

Model C further included 4 narrow emission lines, required by the data, and compatible with being the OVII triplet and the OVIII K_α line. The best fit values of the parameters of the ionized absorber for model C (and for all models tested) are shown in Table 2. The continuum parameters and the goodness of all the models tested are reported in Table 1. This fit, though acceptable ($\chi_\nu^2=1.16$ for 410 d.o.f.), still leaves the presence of residuals due to absorption. This is consistent with the findings by K05, who reported that two absorption components were required to fit the data.

To test the presence of this second absorber, we further added to model C a second PHASE absorbing component. Model D ($\chi_\nu^2=1.12$ for 407 d.o.f.) significantly changed the

⁴We note, however, that the value of this parameter has little effect on our results. For instance, a test using a value of 100 km s^{-1} for this velocity gives values for the free parameters fully consistent (within 1σ) with those obtained in our models.

⁵During the *XMM-Newton* observation the X-ray spectral properties of the source were strikingly similar to those of the 2001 *Chandra* observation (see §4). It is well known that the absorbing properties of the gas in the X-ray region weakly depend on the shape of the SED below 0.1 keV (Netzer 1996; Steenbrugge et al. 2003). This justifies using the same SED used by K05, which provides a direct comparison between models, rather than constraining the UV shape of the SED using the optical monitor (OM) data of the *XMM-Newton* observation.

fit with respect to a single absorber. An F-test gives a probability $\approx 99.9\%$ for the presence of the second absorbing component.

The low ionization absorbing component found in the *XMM-Newton* spectra of NGC 985 (hereafter low-ionization phase or LIP) can be clearly identified by its characteristic absorption by the Fe M-shell (Fe-VII-XIII) unresolved transition array (hereafter UTA, see Behar et al. 2001), and by the presence of the O VII resonant line at ~ 18.6 Å. This component should also produce absorption by charge states like O VI, N VI, and C VI. Lines by these ions are not clearly detected in the spectrum. However, our model does include them, and the data is consistent with their presence (see also §3.3.2). The high ionization absorbing component (high-ionization phase or HIP) is detected by several Fe L-shell charge states, in particular by Fe XVII-XXII.

Few sources show the presence of a very high ionization absorbing component (e.g. NGC 3783, Netzer et al. 2003; NGC 5548, Steenbrugge et al. 2005). K05 suggested the presence of such a component in NGC 985, but reported that it could not be constrained with the *Chandra* data. Thus, we further added a third ionized absorber to our fits (model E), to test the possible presence of this component. Model E improves by $\Delta\chi^2=18$ over model D, for a difference of 3 d.o.f (the ionization parameter, column density, and outflow velocity of the third absorber). According to an F-test this difference is significant (significance $\sim 99.9\%$).

The ionization parameter and column density of the LIP remain consistent within 1σ between this fit and model D. However, the ionization parameter of the HIP decreases by a factor ~ 0.60 , and the column density of this component decreases by a factor ~ 0.42 . The leading charge states of the HIP in model E are then Fe XVII-XX. In turn, the leading charge states of the 3rd, hottest component (hereafter super-hot ionization phase, or SHIP) are Fe XX-XXII (the leading charge states of the LIP are the same ones listed above, as the ionization state of this component did not vary from model D to model E).

3.3. A Global fit to the Spectra

Finally, we analyzed the *RGS* and *EPIC* data simultaneously over the whole energy band. Based on the results obtained for the independent analysis performed for *EPIC* and *RGS*, we fit the spectra (model F) with a power law and a black body component absorbed by three phases of ionized material (LIP, HIP and SHIP), plus the four narrow emission lines detected in the *RGS*, and the Fe line detected with *EPIC*. We forced the photon index of the power law and the temperature of the blackbody to be the same in all the models for all the instruments, but allowed the normalizations to vary freely among spectra from

different detectors. The outflow velocities were fixed to the best fitting values found for the models performed only to the *RGS* data. The parameters for this model are presented in Tables 1 and 2. The parameters of the four narrow emission lines (OVII triplet and OVIII $K\alpha$) modeled are collated in Table 3. Figures 2, 3, and 4 present data and best fit model for the *RGS1*, *RGS2*, and *EPIC-pn*, respectively.

This fit ($\chi^2_\nu=1.25$ for 648 d.o.f.) produced values for the ionized absorbers fully consistent with those derived in model E. However, the photon index among the different fits do vary in a significant way. This is due to the high energy cut off of the *RGS* being below 2 keV, which does not provide a sufficient baseline to constrain this parameter well. It is interesting to note that the continuum parameters for our final model are consistent with those reported for this object by K05, indicating no change in the spectral shape of the source during the two observations.

3.3.1. Continuum Fits

While model E is acceptable over the whole spectrum, in the spectral region between 17 and 21 Å there is a clear excess of flux, of about 10% in the data with respect to the model⁶. This excess, which is present in both the RGS and EPIC data, can be modeled (using an empirical approach) by adding to model E a broad Gaussian component ($\chi^2_\nu=1.21$ for 645 d.o.f.). This broad component, with position at 20.1 ± 0.6 Å, and $\text{FWHM} \sim 7.7 \pm 1.2 \times 10^4$ km s⁻¹, is required by the data with a confidence level of 99.99% (according to an F-test). The width, and position of the line are clearly not consistent with an origin in the Broad Line Region of the source. On the other hand, considering the effect of the ionized absorber below 19 Å, the excess could be produced by a relativistic O VIII $K\alpha$ emission line (e.g. Branduardi-Raymont et al. 2001, Ogle et al. 2004). However, the quality of the data is not good enough to further test this idea. Whatever the nature of this emission, we note that it has no effect on the results presented here for the ionized absorber. The parameters obtained for the absorbing components including this broad feature are fully consistent with those found in Model E.

⁶There is also an overprediction of the model between 15.8 and 16.8 Å, in the region where the UTA is located, which is likely produced by the use of the abbreviated data of the Fe M-shell transitions that produce the UTA (Behar et al. 2001) in our model, see Krongold et al. (2003) for details.

3.3.2. Absorption and Emission Blending

From Figures 2 and 3 it can be observed that, in the regions where the OVII and OVIII emission lines are located, the model predictions are in good agreement with the data. However, while a visual inspection to these spectral regions shows that the emission lines are barely present in the data, Table 3 indicates that they are detected with high significance. This effect is the result of a strong filling of the absorption lines by the emission features. Indeed, the spectra do not show the presence of absorption lines at ~ 18.9 Å, ~ 21.6 Å, and 22.1 Å, where the OVIII K α , OVII K α , and a strong OVI absorption lines are located. Yet, these three lines are black saturated in our models. In addition, the OVII K β absorption line at 18.6 Å is detected in the data, which means that the K α transition should also be present. This further supports the idea of emission and absorption line blending.

4. Absorber Discussion

4.1. A Static Outflow in Photoionization Equilibrium

The ionized absorber found in NGC 985 shows similar characteristics to WAs found in other systems, i.e. the presence of 2 or 3 different ionization components, with increasing column density as the ionization level increases. We note that the 2 absorber best fit model (model D) found for the *XMM-Newton* data is strikingly similar to the one found for the *Chandra* data. Comparing the best fit ionization parameters for the HIP and the LIP of model D with those found by K05 in the *Chandra* data, it is observed that the values are consistent with each other within 1σ . The column densities are also consistent within 2σ . We also note that the ionizing flux level of NGC 985 during the *Chandra* and *XMM-Newton* observations is very similar ($F(0.1 - 10\text{keV}) = 1.2 \pm 0.2 \times 10^{-11} \text{ erg s}^{-1} \text{ cm}^{-2}$ during the first observation and $F(0.1 - 10\text{keV}) = 1.46 \pm 0.21 \times 10^{-11} \text{ erg s}^{-1} \text{ cm}^{-2}$ during the latter one). In addition, the continuum also has indistinguishable parameters during the two observations, with similar photon indexes and blackbody temperatures. This gives us a justification for the use of the same SED between our models and those presented by K05.

The fact that the spectral shape and continuum level of NGC 985 is the same between the two observations, together with the finding of consistent ionization parameters in both spectra strongly suggests that the absorbing components in this object are in photoionization equilibrium. In turn, the lack of significant changes in the column density of the components suggests that we are looking at a static outflow, that has not undergone significant changes in the ~ 1 yr elapsed between the *Chandra* and *XMM-Newton* observations, and probably within the ~ 4 yr between the *BEPOSAX* (also analyzed by K05) and the *XMM-Newton*

observations.

4.2. The 3rd, Hottest, Ionization Absorbing Component

The *XMM-Newton* data shows that the high ionization component can de-blend into two components (HIP and SHIP). We visually searched for, but could not identify, a discrete absorption feature that could show in a significant way the presence of this component in the *RGS* spectra. The improvement in the fit when this absorber is included is produced by differences smaller than 1σ integrated over the whole spectrum. Despite being unobservable by eye, this component appears to be well constrained, as shown in Figure 5, where 1, 2 and 3σ confidence regions for the physical parameters of this absorber are presented.

We notice that the limited S/N of the *Chandra* data of the NGC 985 spectrum was not enough for the detection of this absorbing component. Actually, the SHIP is substantially different from the component hinted by the *Chandra* data. That component was suggested by small residuals between 1.6 and 1.8 Å, where absorption by Fe XXIV to Fe XXVI could be expected. Instead, the higher S/N of the *XMM-Newton* data in this region (through the *EPIC-pn*) allows us to rule out such a component, as no absorption lines by such charge states are detected (see Fig. 6). We set equivalent width 2σ upper limits of 5.3, 3.6 and 2.5 mÅ to the presence of absorption by Fe XXIV, Fe XXV, and Fe XXVI, respectively. However, the presence of gas with even higher ionization is still possible. In Figure 7 we present 1, 2, and 3σ contour plots for the presence of an extremely highly ionized absorbing component in NGC 985 (with ionization even larger than the SHIP and that expected from the *Chandra* data). The presence of such material cannot be ruled out, as is formed by almost entirely stripped gas and thus is almost transparent (for atomic absorption) to the impinging radiation.

4.3. On the Nature of the Absorber: A Multi-Phase Medium

K05 reported that the two absorbing components detected in the *Chandra* data have the same value of the pressure, and thus, if located at the same distance from the ionizing source, could form a single medium in pressure equilibrium. One component could then be confining the other, or a third hotter component could be confining the two detected ones. This result is confirmed by our analysis of the *XMM-Newton* data. Figure 8 presents the thermal photoionization equilibrium curve (or S-curve, Krolik et al. 1981) for the SED used in our analysis. The S-curve marks the points of thermal equilibrium in the T vs. U/T plane,

where T is the photoionization equilibrium temperature of the gas, and U/T is a quantity inversely proportional to the pressure of the gas (see Komossa & Mathur, 2001, and K05 for a detailed explanation of this curve). As can be observed in Figure 8a, the best-fit two absorbing components of model D (HIP and LIP) have very different temperatures, but lie very close to each other in the U/T axis, implying very similar pressures. In fact the gas pressures of the two components are indistinguishable within 1σ .

However, it is interesting to note that the HIP in model D, as well as the HIP found for both *Chandra* and *BEPPOSAX* spectra of NGC 985 by K05, lie close to, but out of the region of thermal stability in the S-curve. Gas in regions of the curve with negative derivative is unstable because any isobaric perturbation will be amplified, leading to net cooling or heating. Thus, the HIP should not be able to survive in this unstable region of the S-curve for periods of time longer than the hydrodynamic timescale of the system t_H (i.e. the timescale in which the medium adapts to mechanical perturbations). K05 points out that, if the different ionization components form truly a multi-phase medium, then t_H must be shorter than the photoionization equilibrium timescale t_{ph} (i.e. the timescale in which the system can adapt to changes in the ionizing continuum). Otherwise, the pressure balance between the phases could be easily broken and the phases would dissolve (see detailed discussion in §5.5 of K05). Since the gas forming the warm absorber of NGC 985 is most likely in photoionization equilibrium (§4.1 and K05) this implies short t_{ph} , and thus short t_H . This presents a serious problem for the existence of the HIP, as the gas that forms it should go rapidly to stable regions of the S-curve (the HIP should dissolve during the 1 year elapsed between the *Chandra* and *XMM-Newton* observations). One possible (though unlikely) explanation could be that the ionization parameter (and thus the temperature) of the HIP has been systematically underestimated in all the analyses of the X-ray spectra of this source, and that this component really lies on the intermediate branch of stability. Another explanation is that the crossing time of the phases through our line of sight is $\ll t_H$, and we always see the phases before they dissolve.

Another explanation that relaxes the above relation between the crossing time and t_H arises from the possible presence of the third higher ionization component (the SHIP) detected only with the larger S/N of the *XMM-Newton* data (Models E and F). Figure 8b shows the location in the thermal equilibrium curve of the 3 absorbing components found in Model F. The pressure of the 3 phases is again indistinguishable within 1σ , however, in this case all 3 components lie in thermally stable regions of the ‘S-curve.’ This 3-phase solution allows the phases to co-exist for long periods of time, even if t_H is small (for instance if the confined phases are composed of small cloudets, as suggested by K05). This is consistent with the finding that the 3 absorbing components have indistinguishable kinematics (the outflow velocity of the 3 phases is consistent with a single value well within 1σ , see Table 2).

This indistinguishable kinematics would further prevent the confined phases to be rapidly destroyed by drag forces (which depend on the relative velocity among the phases). These results support the idea that warm (ionized) absorbers in AGN are formed by a multi-phase medium in pressure equilibrium, with one hot component confining the others. In this case, the different phases of the multi-phase medium could form easily, as the gas tends to go to the stable branches of the thermal equilibrium curve, while keeping pressure balance between them.

WA in other Seyfert 1s also show different phases, in pressure balance (e.g. NGC 3783 Krongold et al. 2003; Netzer et al. 2003; Mrk 279 Fields et al. 2007, though see Constantini et al. 2007). An obvious requirement for the phases to form a single medium, is that they should lie in the same location, i.e. they should be at the same distance from the ionizing source. We have no means to constrain the location of the absorbing components in NGC 985 with the present data. However, we note that, using time-evolving photoionization arguments, Krongold et al. (2007) found that the 2 phases in the ionized absorber in NGC 4051 are consistent with being co-located and in pressure equilibrium.

Our analysis does not seem to favor a continuous radial range of ionization structures. As shown in Figure 9, the data rules out the presence of significant absorption by Fe I-VI. The lack of gas with lower ionization state is further evidenced by the non-detection of O I-V. We find a 2σ upper limit of 17 mÅ for the EW of the O V 22.37 Å transition. This implies a ionic column density $< 7 \times 10^{15} \text{ cm}^{-2}$, a factor ≈ 85 and ≈ 20 lower than those inferred (from our model) for O VII and O VI, respectively (and consistent with the O V column density predicted in our model). From Figure 9 it can also be observed that the data is inconsistent with absorption by Fe XIV-Fe XVI. Thus, at least the LIP seems to be a genuine discrete component. The situation for the HIP and SHIP is more complex, as the ionization parameters of these components are separated only by a factor ≈ 5 . To test whether these two components could be better reproduced by more components (indicating the possible presence of a continuous radial flow for the high ionization gas), we modeled the data adding a fourth ionization component with ionization parameter between those of the HIP and SHIP. The fit showed that this component was not required by the data, further suggesting discrete phases (we set a 2σ upper limit of $1.3 \times 10^{20} \text{ cm}^{-2}$ for the column of this fourth absorber). These results are consistent with the findings by K05 who, based on variability, ruled out a continuous radial flow. The idea of a continuous radial range of ionization structures is recurrent in the literature (e.g. Steenbrugge et al. 2005; Ogle et al. 2004) as it can explain, with a single outflow, both the presence of the warm absorber in Seyfert 1 galaxies and the presence of extended emission produced by highly ionized gas in Seyfert 2 galaxies (Kinkhabwala et al. 2002). However, a multi-phase medium is also consistent with the idea of a single outflow, but detected in emission and absorption at

different locations (see Krongold et al. 2007 for details).

Our results further support a compact absorber. Combined with strong evidence from the UV data for perpendicular motion with respect to our line of sight is several UV absorption systems in other objects (Mathur et al. 1995; Crenshaw et al. 2003; Arav et al. 2004), this strongly suggests that we are looking the flow in a transverse direction, rather than directly in the direction of the flow. This is consistent with a bi-conical structure for quasar winds (e.g. Elvis 2000).

5. Conclusions

The *XMM-Newton* data of NGC 985 shows the presence of an ionized (warm) absorber in the X-ray spectra of this source. The data can be modeled with two or maybe three absorbing components. The presence of a third absorber is statistically significant in the models, however we could not identify a discrete significant absorption feature required by this component (and not modeled with only two absorbers). Therefore, we consider the detection of this component as tentative. The absorbing components (whether two or three different absorbers are present) are in pressure balance (within 1σ) and have outflow velocities indistinguishable from each other. Thus, our results give further support to the idea that ionized absorbers in AGN form a multi-phase medium, where a hot gas component is confining the other(s). However, in the model with only two absorbers, one is located in an unstable branch of this curve. On the other hand, in the three-phase model all the components lie in stable regions of the thermal equilibrium curve. Thus, only the model with three absorbing components allows a multi-phase absorber to survive for long periods of time. In this case, the multi-phase medium would not dissolve even if the crossing time is much larger than the timescale in which the medium adapts to mechanical perturbations.

We thank the referee for constructive comments that helped to improve the paper. This research is based on observations obtained with XMM-Newton, an ESA science mission with instruments and contributions directly funded by ESA Member States and NASA. This work was supported by the UNAM PAPIIT grant IN118905 and the CONACyT grant J-49594. EJB and MSLI have been supported by Spanish MEC under grant AYA2001-3939-C03-02. YK and EJB acknowledge support by the ESA faculty program.

REFERENCES

- Arav, N. 2002, X-ray Spectroscopy of AGN with Chandra and XMM-Newton, MPE Report 279, 153
- Arav, N. 2004, ASP Conf. Ser. 311: AGN Physics with the Sloan Digital Sky Survey, 311, 213
- Arribas, S., Mediavilla, E., del Burgo, C., & García-Lorenzo, B. 1999, ApJ, 511, 680
- Behar, E., Sako, M., & Kahn, S. M. 2001, ApJ, 563, 497
- Behar, E., Rasmussen, A. P., Blustin, A. J., Sako, M., Kahn, S. M., Kaastra, J. S., Branduardi-Raymont, G., & Steenbrugge, K. C. 2003, ApJ, 598, 232
- Blustin, A. J., Page, M. J., Fuerst, S. V., Branduardi-Raymont, G., & Ashton, C. E. 2005, A&A, 431, 111
- Brandt, W. N., Fabian, A. C., Nandra, K., Reynolds, C. S., & Brinkmann, W. 1994, MNRAS, 271, 958
- Branduardi-Raymont, G., Sako, M., Kahn, S. M., Brinkman, A. C., Kaastra, J. S., & Page, M. J. 2001, A&A, 365, L140
- Costantini, E., et al. 2007, A&A, 461, 121
- Crenshaw, D. M., Kraemer, S. B., & George, I. M. 2003, A&A Rev., 41, 117
- Elvis, M. 2000, ApJ, 545, 63
- Fields, D. L., Mathur, S., Pogge, R. W., Nicastro, F., Komossa, S., & Krongold, Y. 2005, ApJ, 634, 928
- Fields, D. L., Mathur, S., Krongold, Y., Williams, R., & Nicastro, F. 2007, ApJ, 666, 828
- Freeman, P., Doe, S., & Siemiginowska, A. 2001, Proc. SPIE, 4477, 76
- Gabriel, C., et al. 2004, Astronomical Data Analysis Software and Systems (ADASS) XIII, 314, 759
- George, I. M., Turner, T. J., Netzer, H., Nandra, K., Mushotzky, R. F., & Yaqoob, T. 1998, ApJS, 114, 73–339, 937
- Grevesse, N., & Noels, A. 1993, in Origin and Evolution of the Elements, p. 15

- Halpern, J. P. 1982, Ph.D. Thesis Harvard University, Cambridge, MA.
- Haro-Corzo, S. A. R., Binette, L., Krongold, Y., Benitez, E., Humphrey, A., Nicastro, F., & Rodríguez-Martínez, M. 2007, *ApJ*, 662, 145
- Jansen, F., et al. 2001, *A&A*, 365, L1
- Jiménez-Bailón, E., Piconcelli, E., Guainazzi, M., Schartel, N., Rodríguez-Pascual, P. M., & Santos-Lleó, M. 2005, *A&A*, 435, 449
- Kaastra, J. S., et al. 2004, *A&A*, 428, 57
- Kinkhabwala, A., et al. 2002, *ApJ*, 575, 732
- Komossa, S., & Mathur, S. 2001, *A&A*, 374, 914
- Kraemer, S. B., Ferland, G. J., & Gabel, J. R. 2004, *ApJ*, 604, 556
- Krolik, J. H., McKee, C. F., & Tarter, C. B. 1981, *ApJ*, 249, 422
- Krolik, J. H. & Kriss, G. A. 2001, *ApJ*, 561, 684
- Krongold, Y., Nicastro, F., Brickhouse, N.S., Elvis, M., Liedahl D.A. & Mathur, S. 2003, *ApJ*, 597, 832 (K03)
- Krongold, Y., Nicastro, F., Elvis, M., Brickhouse, N. S., Mathur, S., & Zezas, A. 2005, *ApJ*, 620, 165
- Krongold, Y., Nicastro, F., Brickhouse, N. S., Elvis, M., & Mathur, S. 2005b, *ApJ*, 622, 842
- Krongold, Y., Nicastro, F., Elvis, M., Brickhouse, N., Binette, L., Mathur, S., & Jiménez-Bailón, E. 2007, *ApJ*, 659, 1022
- Mathur, S., Elvis, M., & Wilkes, B. 1995, *ApJ*, 452, 230
- Netzer, H. 1996, *ApJ*, 473, 781
- Netzer, H., et al. 2003, *ApJ*, 599, 933
- Netzer, H. 2004, *ApJ*, 604, 551
- Nicastro, F., Fiore, F., Brandt, N., & Reynolds, C. S. 1998, *The Active X-ray Sky: Results from BeppoSAX and RXTE*, 501
- Nicastro, F., Fiore, F., Perola, G. C., & Elvis, M. 1999, *ApJ*, 512, 184

- Ogle, P. M., Mason, K. O., Page, M. J., Salvi, N. J., Cordova, F. A., McHardy, I. M., & Friedhorsky, W. C. 2004, *ApJ*, 606, 151
- Piconcelli, E., Jimenez-Bailón, E., Guainazzi, M., Schartel, N., Rodríguez-Pascual, P. M., & Santos-Lleó, M. 2004, *MNRAS*, 351, 161
- Piconcelli, E., Jimenez-Bailón, E., Guainazzi, M., Schartel, N., Rodríguez-Pascual, P. M., & Santos-Lleó, M. 2005, *A&A*, 432, 15
- Pounds, K. A., Reeves, J. N., Page, K. L., Edelson, R., Matt, G., & Perola, G. C. 2003, *MNRAS*, 341, 953
- Reynolds, C. S. 1997, *MNRAS*, 286, 513
- Róžańska, A., Goosmann, R., Dumont, A.-M., & Czerny, B. 2006, *A&A*, 452, 1
- Stark, A. A., Gammie, C. F., Wilson, R. W., Bally, J., Linke, R. A., Heiles, C., & Hurwitz, M. 1992, *ApJS*, 79, 77
- Steenbrugge, K. C., Kaastra, J. S., de Vries, C. P., & Edelson, R. 2003, *A&A*, 402, 477
- Steenbrugge, K. C., et al. 2005, *A&A*, 434, 569
- Wheaton, W. A., Dunklee, A. L., Jacobsen, A. S., Ling, J. C., Mahoney, W. A., & Radocinski, R. G. 1995, *ApJ*, 438, 322

Table 1. Continuum parameters and goodness of the tested models

M	Power Law		E (keV)	Iron Line		Black Body		WA			Goodness χ^2
	Γ	$A_{\text{pwlw}}^{\text{a}}$		σ (keV)	$A_{\text{Line}}^{\text{b}}$	kT (keV)	A_{BB}^{c}	SH	H	L	
A	1.416 ± 0.015	1.63 ± 0.03	–	–	–	–	–	–	–	–	231 for 174 dof
B	1.450 ± 0.016	1.69 ± 0.04	6.421 ± 0.025	0.14 ± 0.03	$1.86^{+0.30}_{-0.28}$	–	–	–	–	–	161 for 171 dof
C	1.20 ± 0.10	2.33 ± 0.11	–	–	–	0.07 ± 0.03	1.31 ± 0.06	–	–	✓	475 for 410 dof
D	1.71 ± 0.10	3.25 ± 0.25	–	–	–	0.08 ± 0.02	1.52 ± 0.15	–	✓	✓	457 for 407 dof
E	1.73 ± 0.12	3.59 ± 0.19	–	–	–	0.08 ± 0.02	1.72 ± 0.17	✓	✓	✓	439 for 404 dof
F	$1.572^{+0.018}_{-0.012}$	$2.89^{+0.08}_{-0.06}$ (rgs) 1.98 ± 0.09 (pn)	6.42 ± 0.025	0.14 ± 0.03	–	0.09 ± 0.01	1.06 ± 0.08 (rgs) 0.60 ± 0.02 (pn)	✓	✓	✓	810 for 648 dof

^aIn units of 10^{-3} ph s $^{-1}$ cm $^{-2}$ keV $^{-1}$ at 1 keV

^bFlux in units of 10^{-5} ph s $^{-1}$ cm $^{-2}$

^cIn units of 10^{-4} L_{39}/D_{10}^2 , where L_{39} is the source luminosity in units of 10^{39} erg s $^{-1}$ and D_{10} is the distance to the source in units of 10 kpc

Table 2. Ionized absorber parameters of the tested models

Model	Low-Ionization PHASE			High-Ionization PHASE			Super High-Ionization PHASE		
	$\log U$	$\log N_H$	V_{out}	$\log U$	$\log N_H$	V_{out}	$\log U$	$\log N_H$	V_{out}
C				$1.26^{+0.06}_{-0.07}$	21.60 ± 0.12	106 ± 204			
D	$-0.06^{+0.12}_{-0.13}$	21.11 ± 0.09	267 ± 159	1.31 ± 0.12	21.99 ± 0.11	272 ± 149			
E	$-0.04^{+0.30}_{-0.09}$	21.08 ± 0.08	273 ± 134	1.09 ± 0.07	21.61 ± 0.15	296 ± 138	1.75 ± 0.07	22.01 ± 0.18	270 ± 168
F	$0.05^{+0.30}_{-0.16}$	21.08 ± 0.18	273 ± 134^a	1.05 ± 0.06	21.55 ± 0.41	296 ± 138^a	1.72 ± 0.09	21.71 ± 0.21	270 ± 168^a

^aVelocities constrained to the best-fit value obtained for model E

Table 3. Parameters of the emission lines

Line	Rest Wavelength ^a Å	Width km s ⁻¹	Flux ^b
OVIII (K _α)	18.97	650±820	4.9 ^{+4.1} _{-1.7}
OVII (w)	21.60	620±390	3.1 ^{+1.7} _{-1.3}
OVII (x+y)	21.85	740±870	3.6 ^{+1.4} _{-1.2}
OVII (z)	22.107±0.010	730±570	5.9±1.0

^aThe position of the emission lines was constrained to have the same redshift found for the OVII (z) line, which was consistent with the rest frame of NGC 985.

^bIntrinsic flux in units of 10⁻¹⁴ erg s⁻¹ cm⁻².

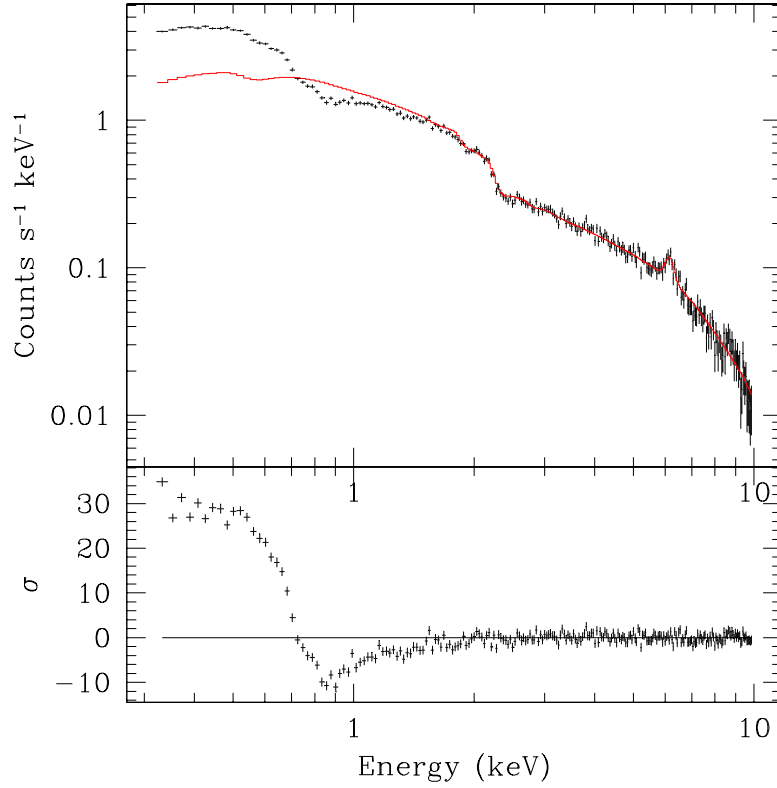


Fig. 1.— *EPIC-pn* spectra of NGC 985. Top panel: Model fit in the 2-10 keV energy band including a continuum power law plus a Fe $K\alpha$ line, attenuated by Galactic absorption. The model (continuous line) has been extrapolated to the whole spectral range. Bottom panel: Residuals to the model. The presence at low energies of absorption by ionized gas, and a soft emission component additional to a simple power law is evident from the data.

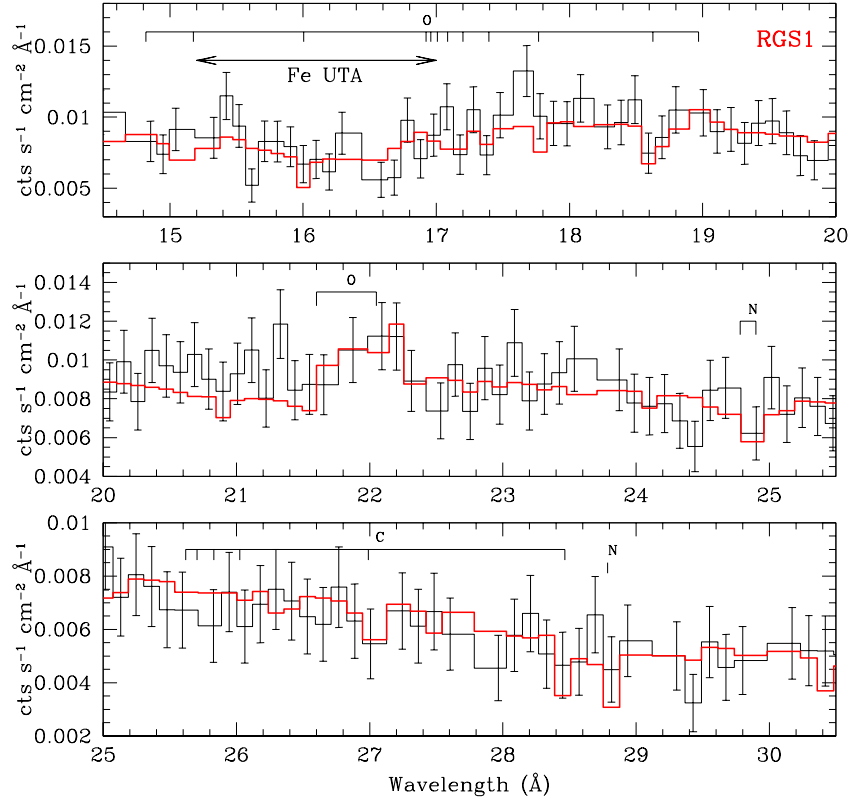


Fig. 2.— Three-phase absorber model plotted against the *RGS1* spectra of NGC 985. The data is presented at the rest frame wavelength of the ionizing absorber. The model (Model F) was produced by fitting simultaneously the *RGS* and *EPIC* spectra.

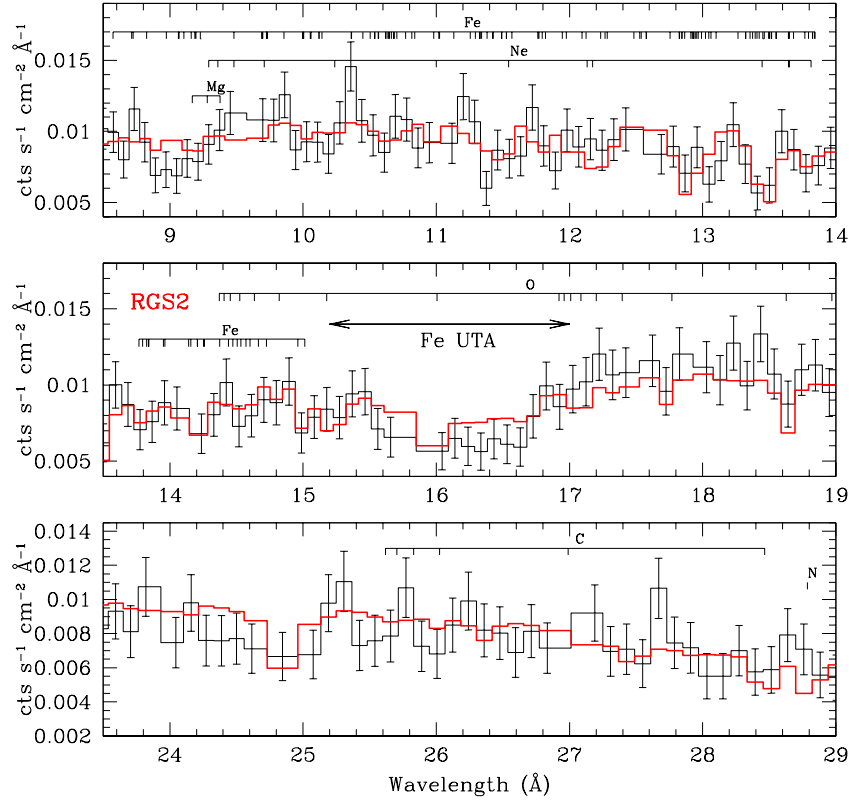


Fig. 3.— Three-phase absorber model plotted against the *RGS2* spectra of NGC 985. The data is presented at the rest frame wavelength of the ionizing absorber. The model (Model F) was produced by fitting simultaneously the *RGS* and *EPIC* spectra.

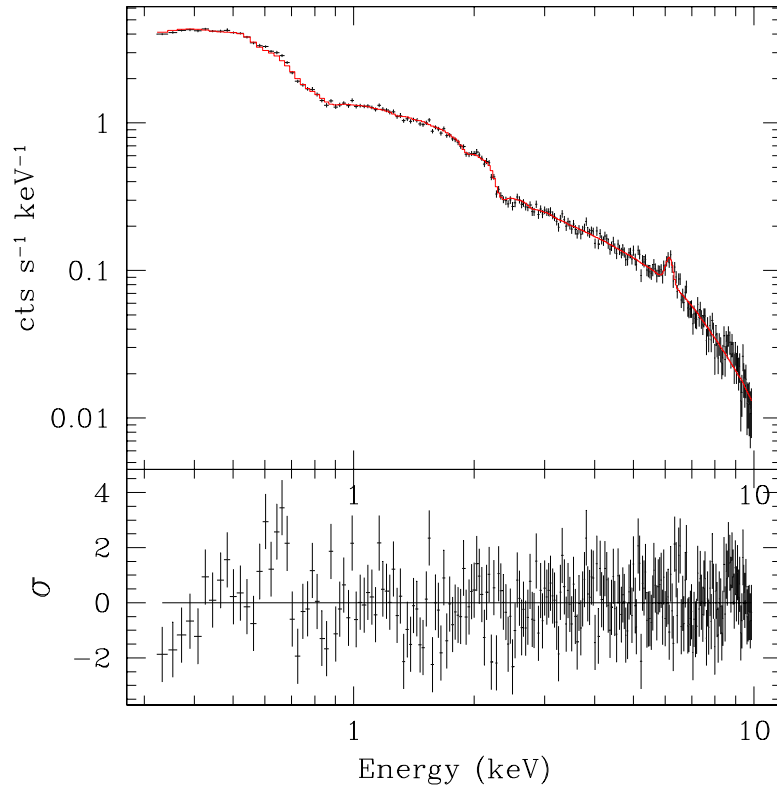


Fig. 4.— Model and residuals of a three-phase absorber model (Model F) over the *EPIC* data of NGC 985. The fit was carried out simultaneously for the *RGS* and the *EPIC* data.

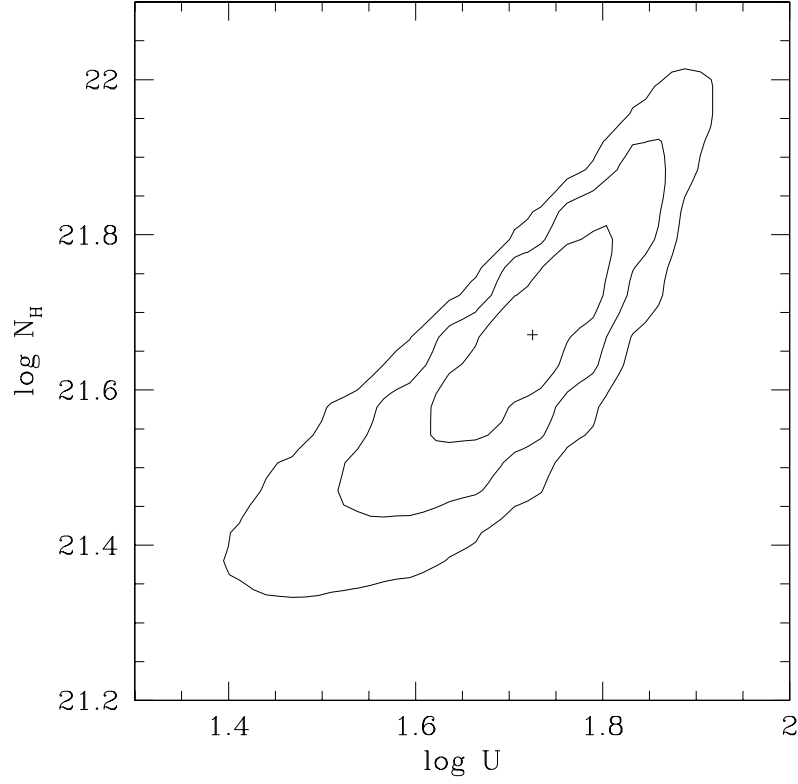


Fig. 5.— Confidence region for the ionization parameter vs. the Hydrogen equivalent column density for the 3rd absorbing component required by the simultaneous fit to the *RGS* and *EPIC* data of NGC 985. The contours represent the 1, 2, and 3 σ confidence levels. Despite the presence of this component cannot be significantly demonstrated by any single absorption line, the parameters of the absorber are well constrained by the data.

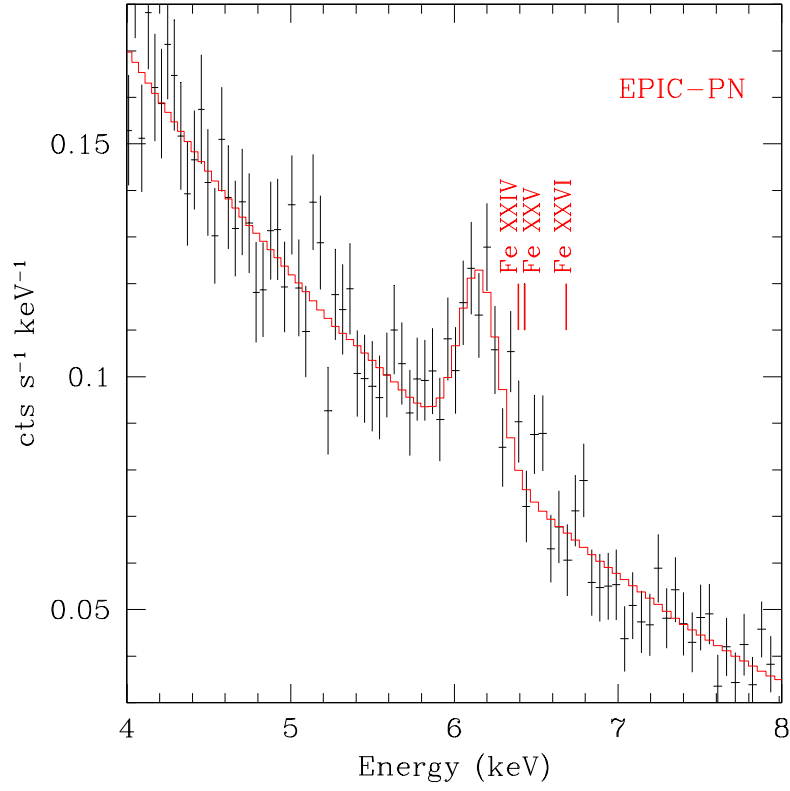


Fig. 6.— Fit to the Fe line region of the *EPIC-pn* spectrum of NGC 985. The labels mark the expected position of absorption lines by highly ionized Fe (Fe XXIV-XXVI). Clearly, no such absorption features are present in the spectrum.

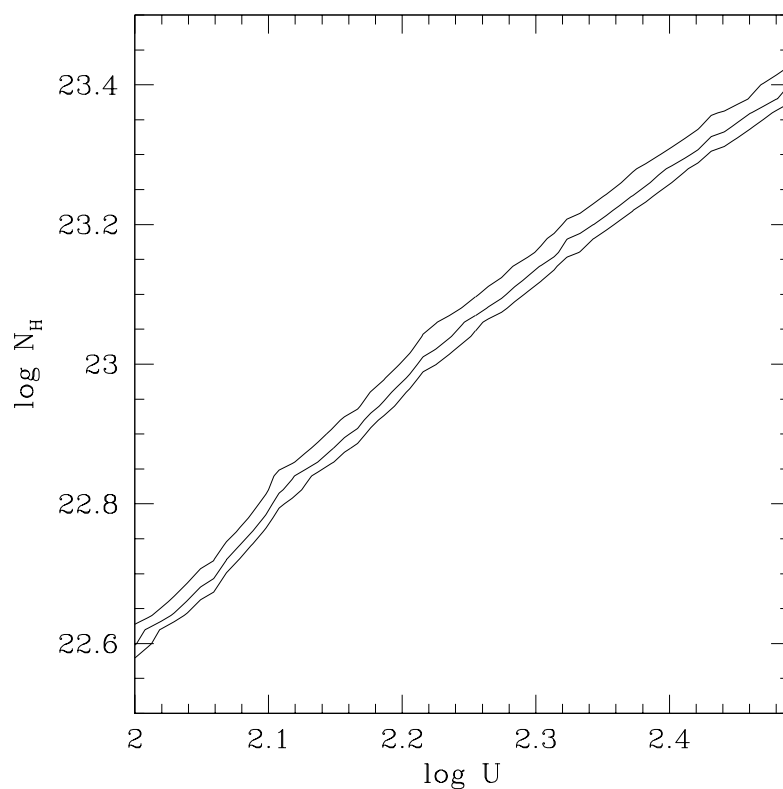


Fig. 7.— Confidence region for the ionization parameter vs. the Hydrogen equivalent column density for a very high ionization absorbing component. The contours represent (from bottom to top) the 1, 2, and 3 σ confidence levels. Such hot gas would be almost transparent to the impinging radiation (as the gas would be almost stripped). The data does not allow us, then, to rule out such an extreme component.

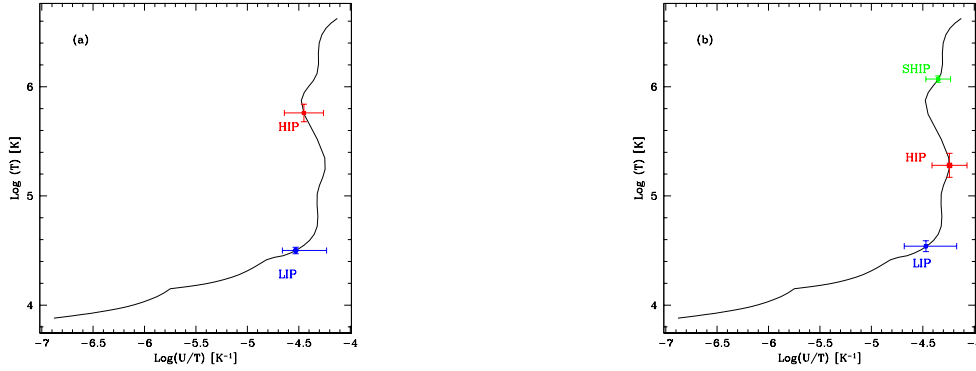


Fig. 8.— Thermal equilibrium curve of the photoionization models used to analyze the data of NGC 985. Panel (a) marks the position of the two-phase absorber model (Model E) in the curve. The two phases are in pressure equilibrium, but the HIP lies in an unstable region of the curve. Panel (b) marks the location of the three phases of Model F. The phases are again in pressure balance, and they all lie in regions of stability. The large positive error bar in the LIP represents the possible effect in the best fit value of $\log U$ induced by the lack of low-temperature dielectronic recombination rates for Fe (e.g. Netzer 2004, Kraemer et al. 2004; see discussion by K05).

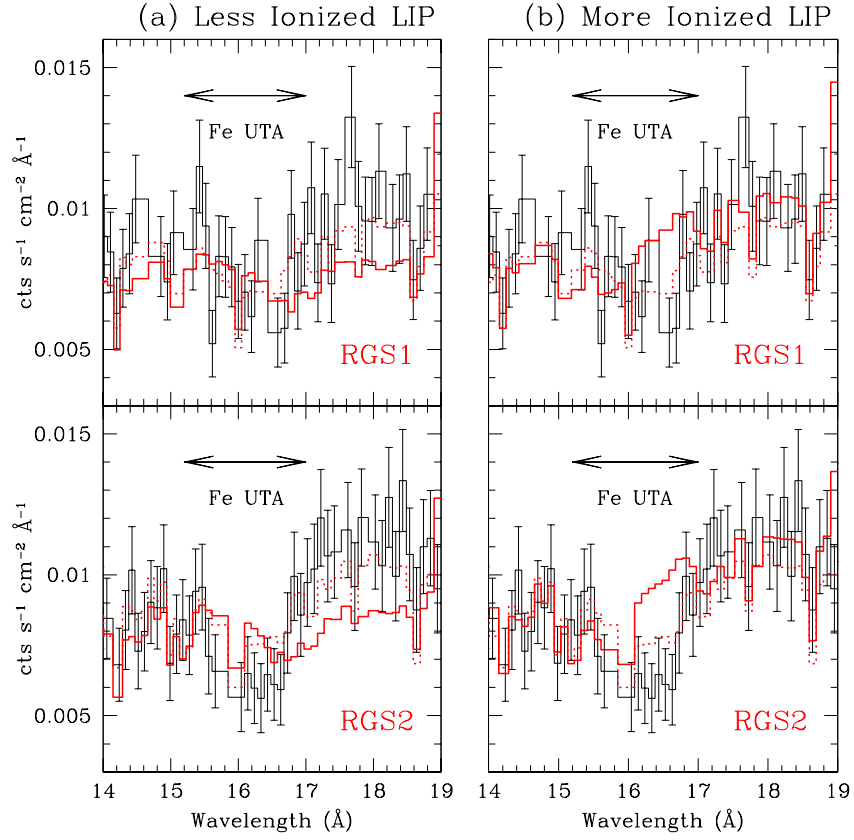


Fig. 9.— LIP models with different value of the ionization parameter. The dotted line shows the best fit model for comparison. (a) Less ionized LIP; $\log(U) = -0.4$. (b) More ionized LIP; $\log(U) = 0.3$.